AJNR

Microstructural Visual Pathway White Matter Alterations in Primary Open-Angle Glaucoma: A Neurite Orientation Dispersion and Density Imaging Study

S. Haykal, A. Invernizzi, J. Carvalho, N.M. Jansonius and F.W. Cornelissen

AJNR Am J Neuroradiol 2022, 43 (5) 756-763
doi: https://doi.org/10.3174/ajnr.A7495
http://www.ajnr.org/content/43/5/756

Microstructural Visual Pathway White Matter Alterations in Primary Open-Angle Glaucoma: A Neurite Orientation Dispersion and Density Imaging Study

S. Haykal, A. Invernizzi, J. Carvalho, N.M. Jansonius, and F.W. Cornelissen

ABSTRACT

BACKGROUND AND PURPOSE: DTI studies of patients with primary open-angle glaucoma have demonstrated that glaucomatous degeneration is not confined to the retina but involves the entire visual pathway. Due to the lack of direct biologic interpretation of DTI parameters, the structural nature of this degeneration is still poorly understood. We used neurite orientation dispersion and density imaging (NODDI) to characterize the microstructural changes in the pregeniculate optic tracts and the postgeniculate optic radiations of patients with primary open-angle glaucoma, to better understand the mechanisms underlying these changes.

MATERIALS AND METHODS: T1- and multishell diffusion-weighted scans were obtained from 23 patients with primary open-angle glaucoma and 29 controls. NODDI parametric maps were produced from the diffusion-weighted scans, and probabilistic tractography was used to track the optic tracts and optic radiations. NODDI parameters were computed for the tracked pathways, and the measures were compared between both groups. The retinal nerve fiber layer thickness and visual field loss were assessed for the patients with glaucoma.

RESULTS: The optic tracts of the patients with glaucoma showed a higher orientation dispersion index and a lower neurite density index compared with the controls ($P < .001$ and $P = .001$, respectively), while their optic radiations showed a higher orientation dispersion index only ($P = .003$).

CONCLUSIONS: The pregeniculate visual pathways of the patients with primary open-angle glaucoma exhibited a loss of both axonal coherence and density, while the postgeniculate pathways exhibited a loss of axonal coherence only. Further longitudinal studies are needed to assess the progression of NODDI alterations in the visual pathways of patients with primary open-angle glaucoma across time.

ABBREVIATIONS: AUC = area under the curve; FA = fractional anisotropy; FISO = fraction of isotropic diffusion; LGN = lateral geniculate nucleus; MD = mean diffusivity; NDI = neurite density index; NODDI = neurite orientation dispersion and density imaging; ODI = orientation dispersion index; OR = optic radiation; OT = optic tract; POAG = primary open-angle glaucoma; RNFL = retinal nerve fiber layer; ROC = receiver operating characteristic; V1 = primary visual cortex; VFMD = visual field mean deviation

Primary open-angle glaucoma (POAG) is a leading cause of irreversible blindness worldwide.[1] It is characterized by the death of retinal ganglion cells, which leads to progressive visual field loss and structural degeneration of the retina.[2] While clinical assessment of POAG remains focused on examining the eye, MR imaging studies of patients with POAG have demonstrated that glaucomatous degeneration spreads downstream from the pregeniculate retinal ganglion cells to the postgeniculate visual pathways through anterograde transsynaptic degeneration, eventually reaching the visual cortex.[3] Specifically, DWI studies have shown evidence of WM degeneration throughout the visual pathways, including the optic tracts (OTs) and optic radiations (ORs).[4-18] However, the underlying pathophysiology of this degeneration is yet to be determined.

Received April 26, 2021; accepted after revision February 26, 2022.

From the Laboratory for Experimental Ophthalmology (S.H., A.I., J.C., F.W.C.) and Department of Ophthalmology (N.M.J.), University of Groningen, University Medical Center Groningen, Groningen, the Netherlands.

S. Haykal, A. Invernizzi, and J. Carvalho received funding from the European Union's Horizon 2020 research and innovation program under the Marie Sklodowska-Curie grant agreements No. 675033 (EGRET-plus), No. 661883 (EGRET-cofund), and No. 641805 (NextGenVis), respectively. S. Haykal, A. Invernizzi, and J. Carvalho were additionally supported by the Graduate School of Medical Sciences, University of Groningen, the Netherlands.

The funding organizations had no role in the design, conduct, analysis, or publication of this research.

Please address correspondence to Shereif Haykal, MD, Laboratory for Experimental Ophthalmology, University Medical Center Groningen, PO Box 30.001, 9700 RB, Groningen, the Netherlands; e-mail: s.a.m.m.haykal@umcg.nl

Indicates open access to non-subscribers at www.ajnr.org

Indicates article with online supplemental data.

http://dx.doi.org/10.3174/ajnr.A7495

Most DWI studies of visual pathway WM degeneration in POAG have relied on the DTI approach to data analysis. DTI uses a tensor to model water diffusion within every voxel, producing parameters such as fractional anisotropy (FA) and mean diffusivity (MD). A decrease of FA and an increase of MD are generally interpreted as an indication of WM structural integrity loss. However, these DTI parameters are nonspecific because they reflect a wide range of WM structural changes, including changes in axonal density, myelination, axonal orientation, and membrane permeability.[19] Higher order biophysical models of DWI have been recently developed to provide more specific and biologically interpretable measures of WM degeneration to address this issue. Neurite orientation dispersion and density imaging (NODDI) is such a higher order biophysical model.[20]

NODDI models water diffusion in the different biologic tissue compartments. It models restricted diffusion in the intraneurite space, hindered diffusion in the extraneurite space, and isotropic diffusion in the CSF.[20] By doing so, NODDI produces 3 parameters: the neurite density index (NDI), the orientation dispersion index (ODI), and the fraction of isotropic diffusion (FISO). NDI indicates the volume fraction occupied by the intraneurite space and thus represents the density of neurites (axons and dendrites) within a voxel. A low NDI is generally associated with a loss of neurites and hence neurodegeneration. ODI indicates the variation of axonal orientation in the extraneurite space and, hence, represents how well-aligned and coherent axons are in a voxel. A high ODI indicates axonal dispersion, while a low ODI indicates axonal coherency. Last, FISO is the volume fraction occupied by CSF in a voxel. A multicompartment model such as NODDI can provide new insights into WM changes occurring in degenerative disorders previously studied exclusively using DTI.

In this study, we present the first application of NODDI to investigate WM changes in POAG, specifically in the pregeniculate OTs and the postgeniculate ORs. By doing so, we aim to characterize the structural nature of these glaucomatous WM changes in terms of axonal density and coherence, to better understand their underlying pathophysiology. Additionally, we assess the diagnostic performance of the NODDI measures of glaucomatous WM degeneration. Finally, for comparison, we use the conventional DTI approach for DWI data analysis.

MATERIALS AND METHODS

Ethics Approval

This study was approved by the Medical Ethical Committee of the University Medical Center Groningen. The study adhered to the tenets of the Declaration of Helsinki. All participants granted written informed consent before participation.

Participants

This study included 2 groups: patients with POAG and healthy controls. Patients with POAG were diagnosed on the basis of having reproducible visual field loss and optic neuropathy consistent with glaucoma in at least 1 eye, accompanied by open angles on gonioscopy. All included patients with POAG were under medical treatment to keep their intraocular pressure within the normal range (≤21 mm Hg). Inclusion criteria for the controls were having intact visual fields, a decimal visual acuity score of 0.8 or higher, and an intraocular pressure of ≤21 mm Hg bilaterally. Exclusion criteria for both groups included having an ophthalmic disorder (other than glaucoma in the POAG group), a history of neurologic or psychiatric disorders, a history of brain surgery, and having an MR imaging contraindication. In total, 23 patients with POAG and 29 controls were included in this study.

Ophthalmic Tests

Visual acuity was tested using a Snellen chart with optimal correction for the viewing distance. Intraocular pressure was measured using a Tonoref Noncontact Tonometer (Nidek). Optical coherence tomography was used to measure the average peripapillary retinal nerve fiber layer (RNFL) thickness using an OCT-HS100 device (Canon Medical Systems). For patients with POAG, visual fields were assessed using a Humphrey Field Analyzer (Carl Zeiss Meditec). A 24-2 test grid was used for 11 patients and a 30-2 grid was used for 12 patients, and the results were expressed as visual field mean deviation (VFMD). For the controls, visual fields were screened for defects using a Humphrey FDT perimeter (Carl Zeiss Meditec) with a C20-1 screening mode (no reproducibly abnormal test locations allowed at $P < .01$).

MR Imaging Data Acquisition

MR imaging data were acquired on a Magnetom Prisma 3T MR imaging scanner (Siemens) with a 64-channel head coil. High-resolution 3D T1-weighted MPRAGE scans were performed using the following parameters: TR = 2300 ms, TE = 2.98 ms, TI = 900 ms, flip angle = 9°, bandwidth = 240 Hz, FOV = 240 × 256 mm^2, voxel size = 1 × 1 × 1 mm, slices per slab = 176. DWI scans were performed using the following parameters: TR = 5500 ms, TE = 85 ms, bandwidth = 2404 Hz, FOV = 210 × 210 mm^2, voxel size = 2.0 × 2.0 × 2.0 mm, number of slices = 66, acceleration factor = 2. DWI data were acquired using a bipolar diffusion scheme at b=1000 s/mm^2 and b=2500 s/mm^2 in 64 noncollinear directions for each shell in an anterior-posterior phase-encoding direction, and 3 images were acquired at b=0 s/mm^2 in both anterior-posterior and posterior-anterior directions to allow correction of susceptibility-induced image artifacts. The acquisition time was around 10 minutes for the T1-weighted scan and 14 minutes for the DWI scan.

MR Imaging Data Preprocessing and Coregistration

DWI data were first denoised using MRtrix3 (www.mrtrix.org).[21,22] Then, the b=0 s/mm^2 images acquired in the anterior-posterior and posterior-anterior phase-encoding directions were used to estimate the susceptibility-induced distortions using the "topup" function of the FMRIB Software Library (FSL v5.0 11, https://fsl.fmrib.ox.ac.uk/fsl). Subsequently, the "eddy" function of FSL (https://fsl.fmrib.ox.ac.uk/fsl/fslwiki/eddy) was used to correct for motion, susceptibility,[23] and eddy current–induced[24] distortions. Finally, rigid body transformation was used to coregister the T1-weighted scan of each participant to the preprocessed DWI scan using the FMRIB Linear Image Registration Tool (FLIRT; http://www.fmrib.ox.ac.uk/fslwiki/FLIRT).[25]

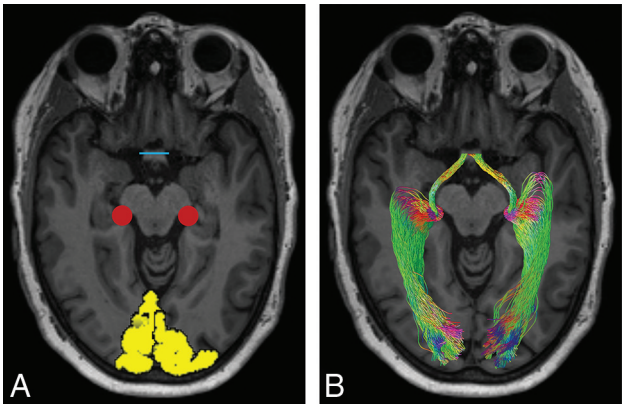

FIG 1. A representative example of visual pathway tractography. *A*, ROI placement overlaid on an axial section of a T1-weighted image. Yellow indicates V1 masks; red, representation of the LGN spherical ROI; blue, the optic chiasm. *B*, Probabilistic OT and OR fiber tracts. Red indicates transverse fibers; green, anterior-posterior fibers; blue, craniocaudal fibers.

Table 1: Demographics and clinical characteristics of participants[a]

	POAG ($n = 23$)	Controls ($n = 29$)	*P* Value
Age (yr)	69.0 (8.5)	66.7 (6.7)	.277
Males	12 (52.2%)	18 (62.1%)	.473
IOP (mm Hg)			
Right eye	13.1 (2.6)	13.0 (2.9)	.947
Left eye	13.1 (3.7)	13.5 (3.3)	.444
Mean	13.1 (2.8)	13.2 (3.0)	.825
RNFL thickness (μm)			
Right eye	69.4 (11.3)	96.9 (8.6)	<.001
Left eye	67.2 (11.5)	97.3 (8.7)	<.001
Mean	68.3 (9.3)	97.1 (7.9)	<.001
VFMD (dB)			
Better eye	−4.0 (5.2)		
Worse eye	−13.0 (9.3)		
Mean	−8.5 (6.0)		

Note:—IOP indicates intraocular pressure.
[a] Values are presented as mean (SD) or number (%).

Visual Pathway Tractography

Unless stated otherwise, all tractography steps were performed using MRtrix3. First, a 5TT image was produced from the coregistered T1-weighted images using FSL commands invoked through MRtrix3.[26,27] 5TT images comprise 5 volumes corresponding to different brain tissues, namely WM, cortical gray matter, subcortical gray matter, CSF, and pathologic tissue. Fiber orientation distributions were then computed from the DWI data for each tissue type using multishell multitissue constrained spherical deconvolution.[28] The produced WM fiber orientation distribution maps were subsequently used for tracking the OTs and the ORs.

The OR fibers were tracked between the lateral geniculate nucleus (LGN) and the primary visual cortex (V1; Fig 1). The LGN was identified manually, and a spherical ROI with a 4-mm radius was used to circumscribe it. The T1-weighted images were automatically segmented and parcellated using FreesSurfer (https://surfer.nmr.mgh.harvard.edu)[29] to produce V1 masks. Probabilistic anatomically constrained tractography[27] was then used to produce a total of 5000 streamlines between the LGN ROI and the V1 mask to delineate the ORs using the following parameters for all subjects: maximum length = 120 mm, minimum length = 70 mm, maximum angle between successive steps = 22.5°, fiber orientation distribution amplitude cutoff value = 0.05.

The OTs were tracked between the LGN and the optic chiasm (Fig 1). The optic chiasm was identified manually, and a rectangular ROI covering its coronal cross-section was created. Due to the small size of the OTs, it was not possible to use anatomically constrained tractography. Instead, we adapted a method originally described for OR tracking to remove anatomically improbable streamlines.[30] First, probabilistic tractography was used to track a total of 50,000 streamlines between the LGN and optic chiasm ROIs using the following parameters for all subjects: maximum length = 50 mm, minimum length = none set, maximum angle between successive steps = 45°, fiber orientation distribution amplitude cutoff value = 0.05. A track density image based on the number of streamlines passing through each voxel was then produced from the streamlines. Subsequently, a threshold was set at the 99th percentile of the intensity distribution of the track density image to exclude voxels containing anatomically improbable streamlines, and a binarized mask was then created from the resulting image. Finally, 500 streamlines were tracked between the LGN and the optic chiasm ROIs using the same parameters described for initially tracking the OTs, while using the thresholded track density image mask to constrain the fiber tracking. All tracked OTs were visually inspected to ensure their anatomic plausibility.

Estimation of NODDI and DTI Parameters

The NODDI model was fitted to the DWI data on a voxel-by-voxel basis using the NODDI Matlab Toolbox (http://mig.cs.ucl.ac.uk/index.php?n=Tutorial.NODDImatlab), producing NDI, ODI, and FISO parameter maps. For comparison, standard DTI parameter maps for FA and MD were computed from the b = 1000 s/mm^2 shell in MRtrix3. Finally, average measures of the NODDI and DTI parameters were computed for the tracked OTs and ORs of each subject.

Statistical Analysis

Demographics and clinical characteristics of patients with POAG and controls were compared using an independent samples t test for parametric continuous variables, a Mann-Whitney U test for nonparametric continuous variables, and a χ^2 test for categoric variables. NODDI and DTI measures of the visual pathways were averaged over both hemispheres and then compared using ANCOVA, including sex and age as nuisance covariates. The results of the clinical eye examinations were averaged over both eyes, and their correlation with NODDI and DTI measures was tested using the Pearson correlation coefficient. Receiver operating characteristic (ROC) curve analysis was used to assess the diagnostic performance of NODDI and DTI measures in discriminating between healthy and glaucomatous visual pathway WM. All statistical analyses were performed using SPSS (Version 25; IBM), and statistical significance was reported at $P < .05$.

Table 2: Comparison of NODDI and DTI measures between patients with POAG and controls[a]

Visual Tract/Parameter	POAG	Controls	Partial η^2	*P* Value
OT				
NDI	0.64 (0.07)	0.70 (0.07)	0.12	.001
ODI	0.21 (0.03)	0.18 (0.02)	0.26	<.001
FISO	0.51 (0.06)	0.49 (0.07)	0.02	.375
FA	0.32 (0.04)	0.39 (0.03)	0.50	<.001
MD	1.55 (0.10)	1.45 (0.11)	0.18	.002
OR				
NDI	0.55 (0.04)	0.57 (0.03)	0.02	.301
ODI	0.17 (0.01)	0.16 (0.01)	0.17	.003
FISO	0.1 3 (0.02)	0.13 (0.02)	0.00	.800
FA	0.51 (0.02)	0.53 (0.02)	0.20	.001
MD	0.8 7 (0.04)	0.85 (0.04)	0.01	.447

[a] Values are presented as mean (SD).

RESULTS

Demographics and Clinical Characteristics

Patients with POAG and the controls did not differ significantly in age, sex, or intraocular pressure. The average RNFL thickness was significantly lower in patients with POAG compared with controls. Details are provided in Table 1.

Differences in NODDI and DTI Parameters between Groups

The OTs of the patients with POAG exhibited lower NDI and FA values and higher ODI and MD values compared with the controls, while the FISO did not differ between the groups. The ORs of the patients with POAG had a higher ODI and FA, while the NDI, FISO, and MD did not differ between the groups. Statistical details and boxplots of the comparisons can be found in Table 2 and Fig 2, respectively.

Correlations with Ophthalmic Measures of Glaucoma Severity

The NDI and FA of the OTs showed a significant positive correlation with VFMD ($r = 0.60$, $P < .005$ and $r = 0.42$, $P < .05$, respectively), while only the FA showed a significant correlation with RNFL thickness ($r = 0.42$, $P < .05$). The ODI, MD, and FISO of the OTs and all tested parameters of the ORs showed no significant correlation with VFMD or RNFL thickness (Online Supplemental Data).

ROC Curve Analysis

`For the OTs, all tested parameters except FISO were able to discriminate between healthy and glaucomatous WM ($P < .05$), with FA having the largest area under the curve (AUC = 0.90). For the ORs, only the ODI and FA were able to discriminate between healthy and glaucomatous WM. ROC curves are shown in Fig 3, and AUC results are listed in Table 3.

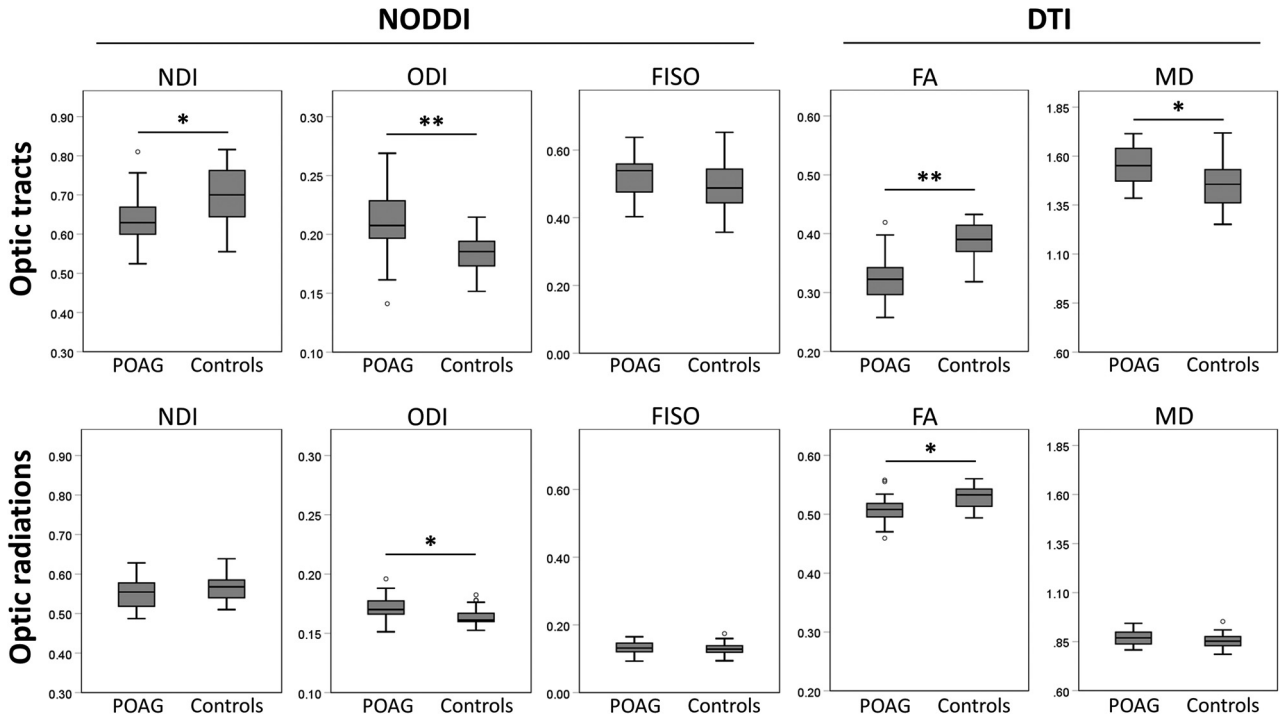

FIG 2. Boxplots showing the distribution of NODDI and DTI measures of the OTs and ORs of patients with POAG and the control group. *Asterisks* indicate a statistically significant difference between groups. The *asterisk* indicates $P < .01$; *double asterisks*, $P < .001$).

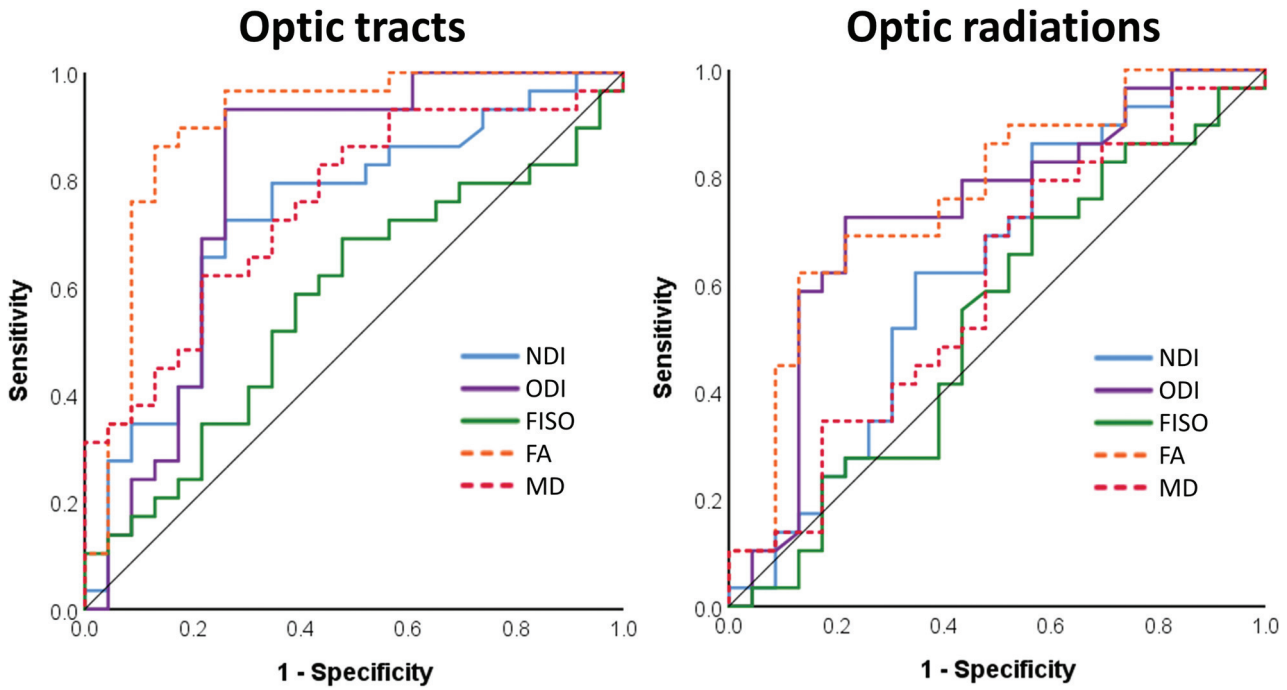

FIG 3. ROC curves assessing the ability of NODDI and DTI measures to discriminate between healthy and glaucomatous visual pathway WM.

Table 3: AUC for NODDI and DTI measures

Visual Tract/Parameter	AUC	95% CI	*P* Value
OT			
NDI	0.73	0.59–0.90	.005
ODI	0.79	0.65–0.93	<.001
FISO	0.57	0.42–0.73	.372
FA	0.90	0.80–1.00	<.001
MD	0.75	0.62–0.88	.002
OR			
NDI	0.63	0.47–0.78	.124
ODI	0.73	0.58–0.87	.005
FISO	0.53	0.37–0.69	.713
FA	0.76	0.62–0.90	.001
MD	0.59	0.44–0.75	.250

DISCUSSION

In this cross-sectional study, we present the first application of NODDI to investigate visual pathway WM degeneration in POAG. We found a disruption of axonal coherence in both the pre- and postgeniculate visual pathways and a loss of axonal density in the pregeniculate pathways only. These findings and their possible interpretations are discussed within the context of current NODDI and transsynaptic degeneration literature.

Pattern of Axonal Density and Coherence Changes in the Visual Pathways of Patients with POAG

The OTs of patients with POAG had a lower NDI and a higher ODI compared with those of controls, implying a loss of both axonal density and coherence. The ORs, on the other hand, showed a higher ODI only, implying a loss of axonal coherence with a preserved axonal density.

The axonal loss found in the OTs is expected because glaucoma causes the death of retinal ganglion cells, the axons of which form the OTs. Evidence of OT axonal loss has also been previously reported in both animal models of glaucoma and patients with POAG.[17,31] However, the lack of OR axonal loss is surprising because previous evidence of LGN[32-35] and visual cortex[36-38] volume loss implies the death of the neurons of the ORs. Because glaucomatous degeneration starts in the pregeniculate pathways and then spreads to the postgeniculate ones, there is a time lag between the degeneration occurring in the OTs and ORs of patients with POAG.[39] This time lag could possibly explain the discrepancy in axonal density changes of the OTs and ORs in our group of patients with POAG.

The loss of OR axonal coherence (as indicated by an increased ODI) in the presence of preserved OR axonal density suggests that disruption of axonal coherence precedes axonal loss in postgeniculate glaucomatous WM degeneration. Indeed, a longitudinal study of anterograde degeneration in an animal model of optic nerve injury found a loss of the "highly coherent appearance" of OR WM preceding axonal loss.[40] Furthermore, a longitudinal NODDI study of patients with stroke found an increase of ODI and no alteration in the NDI in the WM tracts downstream of the stroke lesions at the subacute stage, followed by a decrease in the NDI and a persistently high ODI later at the chronic stage.[41] These findings support the notion that the loss of axonal coherence in the ORs of our patients with POAG is an early sign of postgeniculate WM degeneration.

ODI as a Potential Proxy Marker of Postgeniculate Visual Pathway Demyelination

A study of anterograde transsynaptic degeneration in the visual pathways of both patients with POAG and a glaucoma animal model demonstrated that demyelination of the postgeniculate visual pathways precedes axonal loss.[40] The increase of the ODI and the absence of NDI changes in the ORs of our patients with POAG could potentially be a reflection of the described

postgeniculate demyelination preceding axonal loss. This interpretation is based on the findings of recent NODDI studies of MS. First, a NODDI study of patients with MS found a marked increase of the ODI in active MS lesions in comparison with inactive lesions and normal-appearing WM, suggesting that an increased ODI is a sign of active demyelination.[42] Furthermore, a longitudinal NODDI study of a de- and remyelinating MS animal model reported an increase in ODI during the peak of the demyelination phase, followed by a drop in the ODI during the remyelination phase.[43] Whether the reported increase of the ODI is a direct result of demyelination or a result of other histopathologic changes associated with demyelination is unclear. Nonetheless, the association between active demyelination and increased ODI together with the evidence of demyelination preceding axonal loss in transsynaptic degeneration of the visual pathways suggests that ODI could potentially be a proxy marker of early postgeniculate demyelination.

Comparison to DTI Studies of POAG

We found a loss of FA in both the OTs and ORs of patients with POAG, which is congruent with previous DTI studies of visual pathway WM changes in POAG.[4-16] These findings give the impression that both pre- and postgeniculate visual pathways exhibit the same form of WM degenerative changes, whereas our NODDI findings show that the OTs experience a loss in axonal density and coherence, while the ORs experience a loss in axonal coherence only. Our findings challenge the interpretations of previous DTI studies of POAG and highlight the importance of using biophysical models such as NODDI for studying WM microstructural changes.

Correlations with Ophthalmic Tests of Glaucoma Severity and Diagnostic Performance of NODDI Parameters

Glaucoma severity is commonly assessed over 2 domains: structural and functional. To assess retinal structural glaucomatous degeneration, we measured RNFL thickness using optical coherence tomography, and to assess functional glaucomatous changes, we measured VFMD using a Humphrey Field Analyzer. No correlation was found between the RNFL thickness and any of the tested NODDI parameters. This is surprising because the RNFL is formed of the same retinal ganglion cell axons as the OTs, so a correlation between the NDI of the OTs and the RNFL thickness was expected. Yet, a positive correlation was found between VFMD and the NDI of the OTs. The FA of the OTs showed a significant correlation with both the RNFL thickness and the VFMD, which is in line with findings in previous DTI studies.[11,16]

For the OTs, ROC curve analysis revealed that FA is the best discriminator (AUC = 0.90) of glaucomatous and healthy WM, followed by ODI, MD, and NDI. FA likely surpasses the ODI and NDI in diagnostic ability because the aspects of WM degeneration assessed separately by the ODI and NDI contribute to FA values collectively, producing a larger FA effect size in comparison. This idea is also supported by the results of the ROC curve analysis of the ORs, in which the NDI could not discriminate between glaucomatous and healthy WM, resulting in the FA and ODI AUC values being more comparable (0.76 and 0.73, respectively). While this result makes FA a better binary classifier of glaucomatous WM degeneration, it lacks the biologic interpretability of NODDI parameters. If our suggestion of increased ODI as an early sign of transsynaptic degeneration is accurate, NODDI measures would be more useful in discriminating between healthy WM and different stages of glaucomatous WM degeneration in comparison with DTI measures.

Clinical Implications

Our current findings contribute to the fundamental understanding of the underlying mechanisms of POAG visual pathway degeneration and may also have implications for future glaucoma diagnostics and therapeutics. More specifically, our suggestion of ODI as a marker of early postgeniculate WM degeneration could prove to be useful for early detection of transsynaptic spread of glaucomatous degeneration. Such a marker could play an important role in the development of new glaucoma therapies such as retinal ganglion cell transplantation and neuroprotection, for which assessing the state of the postgeniculate visual pathway would be crucial.

Limitations and Future Directions

A main limitation of this study is the relatively moderate group sizes, which may have contributed to the lack of detectable axonal loss that we found in the ORs of patients with POAG. Furthermore, the inherent limitations of the NODDI approach, specifically its inability to individually assess different crossing fibers within the same voxel, may have influenced our findings. The presence of crossing fibers in the ORs and their absence in the OTs may be partially responsible for the discrepancy in NDI changes that we found between the ORs and the OTs. Future longitudinal NODDI studies of patients with early-stage POAG or a glaucoma animal model are needed to confirm our findings.

CONCLUSIONS

We found that the pregeniculate visual pathways of patients with POAG exhibit a loss of axonal density and coherence, while the postgeniculate pathways exhibit a loss of axonal coherence and a preserved axonal density. Further longitudinal studies are needed to assess the progression of NODDI alterations in the visual pathways of patients with POAG across time.

Disclosures: Shereif Haykal—*RELATED*: *Grant*: European Union's Horizon 2020, *Comments*: European Union's Horizon 2020 research and innovation program under the Marie Sklodowska-Curie grant agreements No. 675033 (EGRET-plus)*; *Fees for Participation in Review Activities such as Data Monitoring Boards, Statistical Analysis, Endpoint Committees, and the Like*: European Union's Horizon 2020, *Comments*: European Union's Horizon 2020 research and innovation program under the Marie Sklodowska-Curie grant agreements No. 675033 (EGRET-plus)*; *Payment for Writing or Reviewing the Manuscript*: European Union's Horizon 2020, *Comments*: European Union's Horizon 2020 research and innovation program under the Marie Sklodowska-Curie grant agreements No. 675033 (EGRET-plus)*; *Provision of Writing Assistance, Medicines, Equipment, or Administrative Support*: European Union's Horizon 2020, *Comments*: European Union's Horizon 2020 research and innovation program under the Marie Sklodowska-Curie grant agreements No. 675033 (EGRET-plus)*; *Other*: Graduate School of Medical Sciences, University of Groningen, the Netherlands, *Comments*: I conducted my work on this study as a PhD student, so I received some financial support from the Graduate School of Medical Sciences at the University of Groningen. Azzurra Invernizzi—*RELATED*: *Grant*: European Union's Horizon 2020, *Comments*: European Union's Horizon 2020 research and innovation program under the Marie Sklodowska-Curie grant agreements No. 661883

(EGRET)*; *Fees for Participation in Review Activities such as Data Monitoring Boards, Statistical Analysis, Endpoint Committees, and the Like*: European Union's Horizon 2020, *Comments*: European Union's Horizon 2020 research and innovation program under the Marie Sklodowska-Curie grant agreements No. 661883 (EGRET)*; *Payment for Writing or Reviewing the Manuscript*: European Union's Horizon 2020, *Comments*: European Union's Horizon 2020 research and innovation program under the Marie Sklodowska-Curie grant agreements No. 661883 (EGRET)*; *Provision of Writing Assistance, Medicines, Equipment, or Administrative Support*: European Union's Horizon 2020, *Comments*: European Union's Horizon 2020 research and innovation program under the Marie Sklodowska-Curie grant agreements No. 661883 (EGRET)*; *Other*: Graduate School of Medical Sciences, University of Groningen, the Netherlands, *Comments*: I collaborated on this study as a PhD student, so I received some financial support from the Graduate School of Medical Sciences at the University of Groningen.* Joana Carvalho—*RELATED*: *Grant*: European Union's Horizon 2020 research and innovation program under the Marie Sklodowska-Curie grant agreement No. 641805 (NextGenVis)*; *UNRELATED*: *Employment*: Champalimaud Center for the Unknown. Nomdo Jansonius—*RELATED*: *Grant*: European Union, Funding: S. Haykal, A. Invernizzi, and J. Carvalho received funding from the European Union's Horizon 2020 research and innovation program under the Marie Sklodowska-Curie grant agreements No. 675033 (EGRET-plus), No. 661883 (EGRET-cofund), and No. 641805 (NextGenVis), respectively. S. Haykal, A. Invernizzi, and J. Carvalho were additionally supported by the Graduate School of Medical Sciences, University of Groningen, the Netherlands. The funding organizations had no role in the design, conduct, analysis, or publication of this research.* Frans Cornelissen—*RELATED*: *Grant*: European Commission, *Comments*: European training grant Egret-plus*; *UNRELATED*: *Grants/Grants Pending*: European Commission/Uitzicht, *Comments*: European Training Grant NexGenVis and Uitzicht-related foundations on visual impairment research financed the costs of some studies. *Money paid to the institution.

REFERENCES

1. Tham YC, Li X, Wong TY, et al. **Global prevalence of glaucoma and projections of glaucoma burden through 2040: a systematic review and meta-analysis.** *Ophthalmology* 2014;121:2081–90 CrossRef Medline
2. Weinreb RN, Khaw PT. **Primary open-angle glaucoma.** *Lancet* 2004;363:1711–20 CrossRef Medline
3. Nuzzi R, Dallorto L, Rolle T. **Changes of visual pathway and brain connectivity in glaucoma: a systematic review.** *Front Neurosci* 2018;12:363 CrossRef Medline
4. Frezzotti P, Giorgio A, Toto F, et al. **Early changes of brain connectivity in primary open angle glaucoma.** *Hum Brain Mapp* 2016;37:4581–96 CrossRef Medline
5. Kaushik M, Graham SL, Wang C, et al. **A topographical relationship between visual field defects and optic radiation changes in glaucoma.** *Investig Ophthalmol Vis Sci* 2014;55:5770–75 CrossRef Medline
6. Sidek S, Ramli N, Rahmat K, et al. **Glaucoma severity affects diffusion tensor imaging (DTI) parameters of the optic nerve and optic radiation.** *Eur J Radiol* 2014;83:1437–41 CrossRef Medline
7. Zikou AK, Kitsos G, Tzarouchi LC, et al. **Voxel-based morphometry and diffusion tensor imaging of the optic pathway in primary open-angle glaucoma: a preliminary study.** *AJNR Am J Neuroradiol* 2012;33:128–34 CrossRef Medline
8. Tellouck L, Durieux M, Coupé P, et al. **Optic radiations microstructural changes in glaucoma and association with severity: a study using 3Tesla-magnetic resonance diffusion tensor imaging.** *Invest Ophthalmol Vis Sci* 2016;57:6539–47 CrossRef Medline
9. Zhou W, Muir ER, Chalfin S, et al. **MRI study of the posterior visual pathways in primary open angle glaucoma.** *J Glaucoma* 2017;26:173–81 CrossRef Medline
10. Nucci C, Mancino R, Martucci A, et al. **3-T diffusion tensor imaging of the optic nerve in subjects with glaucoma: correlation with GDx-VCC, HRT-III and Stratus optical coherence tomography findings.** *Br J Ophthalmol* 2012;96:976–80 CrossRef Medline
11. Chen Z, Lin F, Wang J, et al. **Diffusion tensor magnetic resonance imaging reveals visual pathway damage that correlates with clinical severity in glaucoma.** *Clin Experiment Ophthalmol* 2013;41:43–49 CrossRef Medline
12. Michelson G, Engelhorn T, Wärntges S, et al. **DTI parameters of axonal integrity and demyelination of the optic radiation correlate with glaucoma indices.** *Graefes Arch Clin Exp Ophthalmol* 2013;251:243–53 CrossRef Medline
13. Murai H, Suzuki Y, Kiyosawa M, et al. **Positive correlation between the degree of visual field defect and optic radiation damage in glaucoma patients.** *Jpn J Ophthalmol* 2013;57:257–62 CrossRef Medline
14. Garaci FG, Bolacchi F, Cerulli A, et al. **Optic nerve and optic radiation neurodegeneration in patients with glaucoma: in vivo analysis with 3-T diffusion-tensor MR imaging.** *Radiology* 2009;252:496–501 CrossRef Medline
15. Lu P, Shi L, Du H, et al. **Reduced white matter integrity in primary open-angle glaucoma: A DTI study using tract-based spatial statistics.** *J Neuroradiol* 2013;40:89–93 CrossRef Medline
16. Song X, Puyang Z, Chen A-H, et al. **Diffusion tensor imaging detects microstructural differences of visual pathway in patients with primary open-angle glaucoma and ocular hypertension.** *Front Hum Neurosci* 2018;12:426 CrossRef Medline
17. Haykal S, Curcic-Blake B, Jansonius NM, et al. **Fixel-based analysis of visual pathway white matter in primary open-angle glaucoma.** *Invest Ophthalmol Vis Sci* 2019;60:3803–12 CrossRef Medline
18. Haykal S, Jansonius NM, Cornelissen FW. **Investigating changes in axonal density and morphology of glaucomatous optic nerves using fixel-based analysis.** *Eur J Radiol* 2020;133:109356 CrossRef Medline
19. Jones DK, Knösche TR, Turner R. **White matter integrity, fiber count, and other fallacies: the do's and don'ts of diffusion MRI.** *Neuroimage* 2013;73:239–54 CrossRef Medline
20. Zhang H, Schneider T, Wheeler-Kingshott CA, et al. **NODDI: practical in vivo neurite orientation dispersion and density imaging of the human brain.** *Neuroimage* 2012;61:1000–16 CrossRef Medline
21. Veraart J, Fieremans E, Novikov DS. **Diffusion MRI noise mapping using random matrix theory.** *Magn Reson Med* 2016;76:1582–93 CrossRef Medline
22. Tournier JD, Smith R, Raffelt D, et al. **MRtrix3: a fast, flexible and open software framework for medical image processing and visualisation.** *Neuroimage* 2019;202:116137 CrossRef Medline
23. Andersson JL, Skare S, Ashburner J. **How to correct susceptibility distortions in spin-echo echo-planar images: application to diffusion tensor imaging.** *Neuroimage* 2003;20:870–88 CrossRef Medline
24. Andersson JL, Sotiropoulos SN. **An integrated approach to correction for off-resonance effects and subject movement in diffusion MR imaging.** *Neuroimage* 2016;125:1063–78 CrossRef Medline
25. Jenkinson M, Bannister P, Brady M, et al. **Improved optimization for the robust and accurate linear registration and motion correction of brain images.** *Neuroimage* 2002;17:825–41 CrossRef Medline
26. Zhang Y, Brady M, Smith S. **Segmentation of brain MR images through a hidden Markov random field model and the expectation-maximization algorithm.** *IEEE Trans Med Imaging* 2001;20:45–57 CrossRef Medline
27. Smith RE, Tournier JD, Calamante F, et al. **Anatomically-constrained tractography: improved diffusion MRI streamlines tractography through effective use of anatomical information.** *Neuroimage* 2012;62:1924–38 CrossRef Medline
28. Jeurissen B, Tournier JD, Dhollander T, et al. **Multi-tissue constrained spherical deconvolution for improved analysis of multi-shell diffusion MRI data.** *Neuroimage* 2014;103:411–26 CrossRef Medline
29. Dale AM, Fischl B, Sereno MI. **Cortical surface-based analysis, I: segmentation and surface reconstruction.** *Neuroimage* 1999;9:179–94 CrossRef Medline
30. Martínez-Heras E, Varriano F, Prcõkovska V, et al. **Improved framework for tractography reconstruction of the optic radiation.** *PLoS One* 2015;10:e0137064 CrossRef Medline
31. Ebneter A, Casson RJ, Wood JPM, et al. **Microglial activation in the visual pathway in experimental glaucoma: spatiotemporal characterization and correlation with axonal injury.** *Invest Ophthalmol Vis Sci* 2010;51:6448–60 CrossRef Medline
32. Lee JY, Jeong HJ, Lee JH, et al. **An investigation of lateral geniculate nucleus volume in patients with primary open-angle glaucoma using 7 Tesla magnetic resonance imaging.** *Invest Ophthalmol Vis Sci* 2014;55:3468–76 CrossRef Medline

33. Zhang YQ, Li J, Xu L, et al. **Anterior visual pathway assessment by magnetic resonance imaging in normal-pressure glaucoma.** *Acta Ophthalmol* 2012;90:e295–302 CrossRef Medline
34. Chen Z, Wang J, Lin F, et al. **Correlation between lateral geniculate nucleus atrophy and damage to the optic disc in glaucoma.** *J Neuroradiol* 2013;40:281–87 CrossRef Medline
35. Gupta N, Greenberg G, de Tilly LN, et al. **Atrophy of the lateral geniculate nucleus in human glaucoma detected by magnetic resonance imaging.** *Br J Ophthalmol* 2009;93:56–60 CrossRef Medline
36. Boucard CC, Hernowo AT, Maguire RP, et al. **Changes in cortical grey matter density associated with long-standing retinal visual field defects.** *Brain* 2009;132:1898–1906 CrossRef Medline
37. Zhang S, Wang B, Xie Y, et al. **Retinotopic changes in the gray matter volume and cerebral blood flow in the primary visual cortex of patients with primary open-angle glaucoma.** *Invest Ophthalmol Vis Sci* 2015;56:6171–78 CrossRef Medline
38. Fukuda M, Omodaka K, Tatewaki Y, et al. **Quantitative MRI evaluation of glaucomatous changes in the visual pathway.** *PLoS One* 2018;13:e0197027 CrossRef Medline
39. Haykal S, Jansonius NM, Cornelissen FW. **Progression of visual pathway degeneration in primary open-angle glaucoma: a longitudinal study.** *Front Hum Neurosci* 2021;15:630898–11 CrossRef Medline
40. You Y, Joseph C, Wang C, et al. **Demyelination precedes axonal loss in the transneuronal spread of human neurodegenerative disease.** *Brain* 2019;142:426–42 CrossRef Medline
41. Mastropietro A, Rizzo G, Fontana L, et al. **Microstructural characterization of corticospinal tract in subacute and chronic stroke patients with distal lesions by means of advanced diffusion MRI.** *Neuroradiology* 2019;61:1033–45 CrossRef Medline
42. Sacco S, Caverzasi E, Papinutto N, et al. **Neurite orientation dispersion and density imaging for assessing acute inflammation and lesion evolution in MS.** *AJNR Am J Neuroradiol* 2020;41:2219–26 CrossRef Medline
43. Luo T, Oladosu O, Rawji KS, et al. **Characterizing structural changes with devolving remyelination following experimental demyelination using high angular resolution diffusion MRI and texture analysis.** *J Magn Reson Imaging* 2019;49:1750–59 CrossRef Medline